Journal of Ovonic Research Vol. 21, No. 2, March - April 2025, p. 249 - 262

Green synthesis and characterization of nitrogen doped reduced graphene oxide nanosheets as electrode material for direct ethanol fuel cell

S. Saini [a], V. Sharma [b], M. D. Sharma [a,*]
[a] *Department of Physics, Centre of Advance Study, Panjab University, Chandigarh 160014, India*
[b] *Department of ECE, University Institute of Engineering and Technology, Panjab University, Chandigarh 160014, India*

Nitrogen doped reduced graphene oxide (NRGO) nanosheets are synthesized by electrochemical etching and hydrothermal synthesis techniques. NRGO prepared at different reaction times and nitrogen precursor concentrations are analyzed electrochemically. The optimized sample is then structurally analyzed by X-Ray diffraction (XRD) and Fourier transform infrared spectroscopy (FTIR), and optical properties are studied by Raman Spectroscopy. The structure and morphology are studied using High-resolution transmission electron spectroscopy (HRTEM) and Field emission scanning electron microscopy (FESEM). Thermal stability of the samples is analyzed by Thermogravimetric analysis (TGA). The electrochemical studies reveal the electrocatalytic activity of NRGO for ethanol oxidation, thus making a superior metal-free catalyst for fuel cells.

(Received January 9, 2025; Accepted April 16, 2025)

Keywords: Renewable energy, Fuel cell, Reduced graphene oxide, Electrode materials, Green synthesis

1. Introduction

There are several interconnected environmental challenges the world is facing today: population growth, pollution, global warming, and the green energy requirement. Power is required for daily household activities, transportation, industries, electronic devices, and storage devices [1], [2], [3]. Rapid population growth leads to over consumption of natural resources, causing more pollution and greenhouse gas emissions from industrial activities. Renewable energy transition is crucial for mitigating global warming, enhancing air quality, as well as ensuring future sustainability. Prioritizing green energy and environmental stewardship is vital for our planet's health. Fuel cells (FCs), an electrochemical energy production device, are increasingly becoming a potential green energy source. FCs have been attracting considerable attention because of their capacity to efficiently convert the chemical energy of different fuels into electric energy with utmost efficiency and minimal emissions. FCs can run without releasing pollutants like oxides of nitrogen, carbon, and sulfur, making them an environmentally acceptable power source. They are characterized by several features that make them an attractive technology for the clean and efficient generation of power. High current output density, clean electricity generation, high efficiency, quick response, fuel flexibility, and quiet operation all combine to establish these systems as a sustainable alternative to traditional power generation methods[4]. Therefore, it follows that FCs are suitable for a range of applications ranging from portable (consumer applications such as power supplies for mobile phones or tablet computers; power supply for recreational vehicles or caravans; energy supply for remote sensors with limited access) to stationary (prime power, commercial and residential combined heat and power, and uninterrupted power supply) ones [5].

* Corresponding author: manishdevsharma@yahoo.com
https://doi.org/10.15251/JOR.2025.212.249

In fuel cells, carbon-based materials play a significant role in the operation and efficacy of fuel cells. They principally serve as supports for catalysts to accelerate electrochemical reactions necessary for the fuel cell operation. The importance of carbon materials originates from their large surface area, electrical conductivity, and adjustable porosity required for optimizing the performance of catalysts in the cells. A main use of carbon materials in fuel cells is providing support for metal catalysts, which are essential in oxygen reduction reaction (ORR) and fuel oxidation processes. Carbon black, carbon nanotubes, and graphene provide larger surfaces on which metal nanoparticles can be dispersed, thereby enhancing their overall catalytic activity [6], [7]. Properties such as pore size and morphology of these materials that act as support structures have a significant impact on the electrochemical performance of catalysts. In particular, mesoporous and microporous carbons enhance reactant accessibility to active sites on the catalyst [6], [8]. Moreover, the utilization of functional carbon materials will increase the electrocatalytic activity through optimizing the catalyst-reactant interaction[9]. However, the durability of carbon-based materials at fuel cell operating conditions is a paramount concern. Carbon supports are oxidized, especially at high potentials, and this leads to degradation and loss of catalytic activity [10], [11]. This mechanism is aggravated by fuel cycling, where the metal particles aggregate due to carbon corrosion, resulting in a decrease in their electrochemical surface area (ECSA) [12]. Studies have established that the stability of carbon supports can be advanced by using novel materials such as nitrogen-doped carbon nanotubes, which enhance both their electrocatalytic properties and stability as well [13].

Reduced graphene oxide (rGO) is a vital material in fuel cell electrode development due to its distinctive characteristics that improve the electrochemical efficiency and stability of fuel cells. The integration of rGO into fuel cell designs addresses several important challenges, including the need for efficient electrocatalysts, improved conductivity, and enhanced durability under operational conditions. One of the most significant advantages of rGO is its large surface area that promotes the dispersion of active catalytic materials. This feature is very crucial in optimizing the electrocatalytic activity of fuel cells, especially for ORR and fuel oxidation [14], [15]. The huge theoretical surface area of around 2630 m^2g^{-1} estimated for rGO allows it to have numerous active sites needed for catalytic reactions, thereby improving the overall efficiency of the fuel cells [15]. Moreover, during the process of reducing graphene oxide (GO) to rGO, many functional groups that contain oxygen are eliminated, thus enhancing electronic conductivity, which makes them suitable as electrodes [16]. Apart from being a catalyst support, rGO could also improve the overall architecture of fuel cell electrodes. Inclusion of rGO in electrode materials can increase their mechanical strength and flexibility, an attribute that is important for maintaining structural integrity at different operational conditions [17]. The rGO can aid better contact with electrolyte, hence improved ion transfer and general fuel cell electrochemical performance [16]. Further improvement in the electrochemical properties of rGO can be achieved by doping with other elements such as nitrogen. NRGO has shown improved fuel cell electrocatalysis, particularly in alkaline media, where it enhances ORR[18]. The introduction of nitrogen into the rGO structure creates additional active sites that can participate in the electrochemical reactions, thereby increasing the efficiency of the electrode[18], [19]. This modification not only increases catalytic activity but also helps to ensure the integrity of the electrode material during operations.

The carbon structures are modified by nitrogen doping by hydrothermal method for nitrogen-doped graphene quantum dots in ammonia [20], treatment with nitrogen plasma [21], wet chemical nitrogen doping [22], and solvothermal technique [23]. XPS analysis shows that the nitrogen binding to the carbon structure takes place as three distinct types, namely pyridinic-N, pyrrolic-N, and graphitic-N centers [24], [25], [26]. The electronegativity of nitrogen is higher than compared of carbon; therefore, nitrogen has a tendency to attract electrons from carbon atoms. Thus, nitrogen centers are high in electron density and provide electrons necessary to improve the electrochemical efficiency [20]. Many researchers have synthesized NRGO-supported metal catalysts for fuel cell applications. He et al. [27] used lyophilization-assisted and mild N-doping methods to synthesize NRGO and used it as a catalyst support. Insight from the electrochemical tests reveals that ECSA, electrochemical activity, and oxygen reduction capability of Pt nanoparticles supported on the NRGO are better than those of the regular Pt/GO and Pt/C catalysts. New horizons have been made regarding the role of support in stability enhancing of Pt

nanoparticles because of (1) improved distribution of Pt particles on NRGO, (2) enhanced electrical conductivity, and (3) nitrogen itself acts as a catalyst during ORR when Pt nanoparticles aggregate on NRGO. Kakaei et al. [28] synthesized NRGO nanosheets using the electrochemical method, and Pd nanoparticles were later decorated onto their surface. The synthesized Pd/NRGO shows better electrocatalytic activity for ORR and ethanol oxidation. The reason behind the superior performance of Pd/NRGO is an increase in the ECSA due to nitrogen doping. The membrane electrode assembly (MEA) was fabricated using Pd/NRGO in alkaline direct ethanol fuel cells. The maximum power output obtained is 31.5 mW cm^{-2}.

Emphasis has been put on synthesizing metal-free catalysts because of the degradation of catalysts due to metal agglomeration [29], [30]. Lu et al. [31] have fabricated metal-free NRGO and studied the electrochemical properties. In this study, a simple and cost-effective route is used to synthesize nitrogen-doped reduced graphene oxide (NRGO), which was realized through catalyst-free thermal annealing of 5-aminotetrazole monohydrate (AM). Optimized parameters with the 1:25 ratio of GO to AM and annealing at 700°C, forming NRGO containing approximately up to 10.6% nitrogen content. The NRGO displays a remarkable electrocatalytic performance for ORR in alkaline electrolytes, and it outperforms commercial Pt/C catalysts. Farzaneh et al. [32] studied passive direct methanol fuel cells for cathode electrocatalyst using hydrothermally produced NRGO to be compared with commercial Pt/C. NRGO cathode tolerates higher optimal methanol concentration than the commercial Pt/C, making its performance far exceed that of Pt/C by offering 208% power density, 269% fuel efficiency, and better current stability rate (77%) at the same amount of methanol used. Farzaneh et al. [33] reported the role of the type of N-bonding in the graphitic network in ORR performance. It is noted that at low potentials, the N content enhances the performance irrespective of the bonding configuration; however, at high potentials, pyridinic N content contributes significantly to ORR due to activation of their lone pair of electrons. The inhomogeneous embedding of nitrogen atoms in the graphitic arrays of rGO promotes the formation of numerous defects, which may expose edges and planar sites, thereby increasing the ability of the catalyst to adsorb molecular oxygen for higher ORR activity [34].

In this work, we have synthesized rGO directly from graphite using a one-step electrochemical etching method and NRGO using the hydrothermal synthesis method. Urea is used as a precursor for nitrogen doping. The prepared samples are electrochemically characterized in an alkaline medium, using KOH as electrolyte to check their performance. The structural properties, like morphology and crystallite size, are analyzed through XRD, HRTEM, FE-SEM, and FTIR. The thermal stability of NRGO is examined through TGA. Optical properties and electrochemical properties are also studied for NRGO.

2. Experimental

2.1. Materials

The graphite rods were acquired from SnG Lab Supplies with 99% purity. Lemons were purchased from a local market. Urea ($CO(NH_2)_2$, acetone (C_3H_6O), ethanol (C_2H_5OH), and potassium hydroxide (KOH) were procured from Qualigens Fine Chemicals. All solutions were prepared in deionized (DI) water.

2.2. Synthesis of rGO

The rGO was synthesized by electrochemical etching of graphite rods through a single-step green synthesis method. Two graphite rods, one acting as a cathode and the other as an anode, were connected to a DC regulated power supply. Filtered lemon juice in DI water was used as an electrolyte for the exfoliation of the outer surface of the graphite rod connected to the anode. Citric acid present in the lemon juice acted as the etchant. Figure 1 represents the schematic diagram of the experimental setup used to synthesize rGO. Various reaction settings were optimized by a series of reactions in which one parameter was altered, keeping the rest of the parameters fixed. For each reaction, lemon juice was added to DI water to make a 100 ml solution, and a potential

was applied across the electrodes. The reaction mechanism governing the formation of reduced graphene oxide is as follows:

$$C_6H_8O_7 + 3H_2O \rightarrow C_6H_5O_7^{3-} + 3H_3O^+ \quad (1)$$

In an electrolytic cell, the reduction reaction occurs at the cathode, where electrons are used up to form hydronium ions (H_3O^+) and hydrogen gas or hydroxide ions are released into the solution. Furthermore, water dissociation produced some hydroxide ions. At the anode, nucleophile OH^- ions were interposed into the carbon layers of the graphite rod. The positive charge on the electrode surface attracted negative ions and caused a swelling on the outer layer of the electrode in the form of sheets. These rGO sheets are then settled at the bottom of the cell in the form of black powder. The powdered material is then filtered out and washed multiple times with DI water to filter out ionic impurities. Lastly, the material is dried overnight in an oven at 60˚C [35].

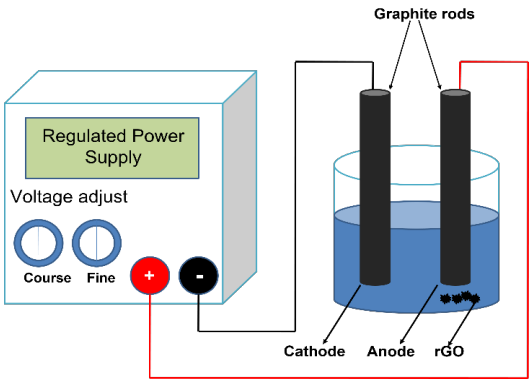

Fig. 1. Experimental setup to synthesize rGO using graphite rods.

2.3. Synthesis of NRGO

NRGO was synthesized using the hydrothermal synthesis method. To synthesize NRGO, 100 mg rGO was mixed with a 100 mM solution of urea, followed by sonication for 15 minutes. The dispersed solution was then shifted into a Teflon-lined 100 ml autoclave and heated in an oven at 150˚C. All the prepared samples were separated using a filter paper and washed with DI water to eliminate the unreacted ionic species. The filtered samples are then transferred into an oven at 80˚C for overnight drying.

2.4. Characterization of NRGO

The synthesized material is structurally characterized using Panalytical X'Pert Pro XRD equipment consisting of theta theta goniometer with a range of $2\theta = 0^{\circ} to\ 160^{\circ}$. The instrument is equipped with a monochromatic Cu-Kα radiation source (1.5406 Å) with Ni metal as beta filter and x'Celerator solid state detector. FTIR is performed using a Bruker Alpha ATR-FTIR spectrophotometer. Raman Spectroscopy is performed using Alpha300RA model using a 532 nm diode pumped solid state laser. The spectrograms are recorded at an output power of 35 mW. TGA is performed on Perkin Elmer STA 6000 from room temperature to 800˚C with a temperature step of 10˚C per minute in an air atmosphere. Morphology of the prepared sample is studied through HRTEM (Jeol; Model: JEM 2100 plus) and FESEM (Hitachi, Japan; Model: SU8010 series).

2.5. Electrochemical characterization of NRGO

The electrochemical characterization has been performed using a three-electrode configuration employing the Autolab type II potentiostat/galvanostat. These materials were tested for cyclic voltammetry (CV) using the synthesized material as the working electrode deposited on a glassy carbon electrode (GCE), counter electrode (platinum wire), and reference electrode (Ag/AgCl). In this case, the electrolyte used is 1M KOH. In order to fabricate the catalyst ink, 10

mg of the prepared sample is mixed with DI water and 100 µL isopropyl alcohol to make the total volume 1 mL. The mixture is ultrasonicated for 60 minutes to obtain a well-dispersed solution. Alumina slurry is used to clean and polish the GCE to remove any adsorbed species. Then, 3 µL of catalyst ink is drop-cast onto the GCE and dried at room temperature before use.

3. Results and discussion

3.1. Optimized reaction conditions for the synthesis of rGO

The prepared rGO samples are optimized by comparing the ratio of D band to G band (I_D/I_G) in Raman spectroscopy, often referred to as the intensity ratio, a very useful tool in determining the degree of functionality expected from reduced graphene oxide (rGO) structures for applications such as fuel cells. The D band observed around 1350 cm^{-1} is due to the presence of defects and disorders in the graphene lattice, while the G band around 1580 cm^{-1} corresponds to the E_{2g} phonon mode of sp^2 hybridized carbon rings. The I_D/I_G ratio reflects the movement of the graphitic planes and the extent of defects within the axes; an increase in the ratio represents increased disorder and a reduction in sp^2 domains. In case of fuel cell application, the I_D/I_G ratio is even more important since it affects the rGO electrical conductance and therefore the electrochemical properties of the material. As such, rGO with a high I_D/I_G ratio is reported to have good electrochemical properties and thus can be used as a prospective material for fuel cell electrodes [36]. The I_D/I_G ratio, which is illustrative of the level of defects in rGO composition, helps in improving the reactivity of the material and the number of active sites available for electrochemical reactions, such as in fuel cells [37].

3.1.1. Variation with applied potential

The rGO nanosheets are prepared by the electrochemical etching method using graphite rods as electrodes and lemon juice solution as electrolyte with application of a constant DC potential. Applied potential plays an important role in finding the number of layers and the percentage of graphitic nature of the material [35]. In the present work, different voltages were applied to prepare three samples, viz 10 V, 12.5 V, and 15 V. Potentials were applied to different electrolytic cells, keeping the reaction time of 3 hours and volume of lemon juice of 10 mL fixed. The three samples prepared are characterized by Raman spectroscopy, and the spectrograms are shown in Figure 2(a). I_D/I_G values for samples prepared at 10 V, 12.5 V, and 15 V are 0.78, 1.01, and 0.90, respectively. The maximum intensity ratio is observed for rGO prepared at 12.5 V.

3.1.2. Variation with reaction time

The effect of reaction time ranging from 2 h-5 h was observed at a fixed potential of 12.5 V and 10 mL of lemon juice in 100 mL solution. At a reaction time of 5 hours, a larger I_D/I_G of 0.93 was achieved (Table 1). This behavior could be attributed to the introduction of defects into the otherwise ideal sp^2 hybridized structure of rGO as the reaction time is increased. Figure 2(b) shows the Raman spectrographs of rGO prepared at different reaction times.

3.1.3. Variation with concentration of electrolyte

In 100 mL of solution, the volume of lemon juice is varied from 5 mL to 25 mL, and separate reactions are allowed to proceed at an applied potential of 12.5 V for 5 hours. The maximum I_D/I_G is observed for the lowest concentration of lemon juice. With an increase in the concentration, a decrease in the intensity ratio is observed. Since the intensity ratio for GO is usually lower than reduced graphene oxide [38], with an increase in the concentration of lemon juice, excessive oxygen-containing functional groups might be attached to the rGO structure, resulting in a decrease in the intensity ratio. Raman spectrographs with concentration variation are shown in Figure 2(c).

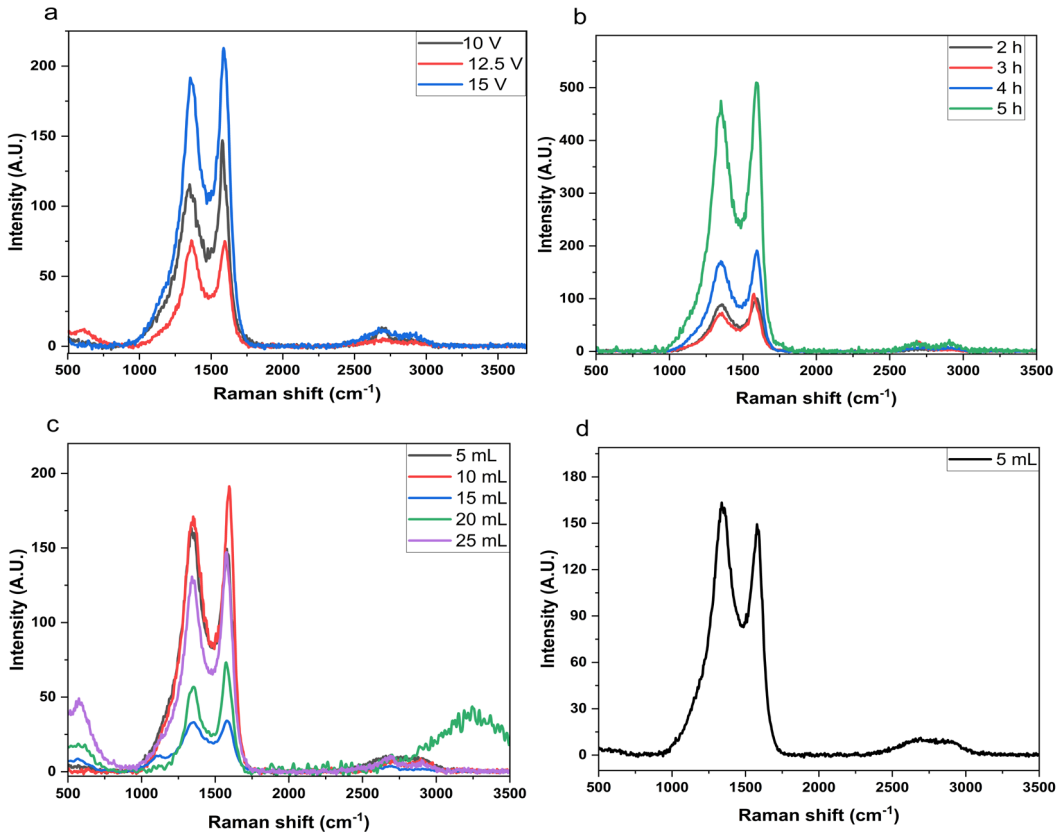

Fig. 2. Raman spectra of rGO showing variation in the intensities of D and G bands with variation in (a) applied potential, (b) reaction time, and (c) concentration of electrolyte (Inset: Raman spectra of rGO prepared using 15 mL lemon juice in electrolyte solution). Variation in one parameter is studied while keeping the other two fixed.

Table 1. Optimization of reaction parameters for the synthesis of rGO.

Voltage Optimization			
Voltage (V)	Reaction time (h)	Volume of lemon juice (mL)	I_D/I_G
10	3	10	0.78
12.5	**3**	**10**	**1.01**
15	3	10	0.90
Time Optimization			
Voltage (V)	Reaction time (h)	Volume of lemon juice (mL)	I_D/I_G
12.5	2	10	0.89
12.5	3	10	0.67
12.5	4	10	0.89
12.5	**5**	**10**	**0.93**
Concentration Optimization			
Voltage (V)	Reaction time (h)	Volume of lemon juice (mL)	I_D/I_G
12.5	**5**	**5**	**1.09**
12.5	5	10	0.97
12.5	5	15	0.89
12.5	5	20	0.78
12.5	5	25	0.88

3.2. Characterization of NRGO

XRD helps to study and analyze the crystal structure and lattice parameters. Pure graphite has a sharp crystalline peak at 2θ~26˚ [39], [40]corresponding to (002) plane, which is shifted to a lower angle (2θ~10˚) for GO due to an increase in the interplanar spacing due to the presence of additional functional groups that contain oxygen [41]. This inverse relation is governed by Bragg's law as shown below:

$$d = \frac{n\lambda}{sin\theta} \tag{2}$$

where d is interplanar spacing, λ is the incident wavelength (1.5406), and θ is the diffraction angle. Since in rGO the oxygen-containing functional groups are reduced, restoration of sp^2 hybridized graphene structure leads to a prominent peak at 2θ = 25.52˚ corresponding to the (002) plane as shown in Figure 3(a). A non-significant peak centered at 43.52° is also observed, which corresponds to the (100) plane. A similar diffractogram is observed for NRGO, showing two peaks centered at 25.89° and 44.68° corresponding to (002) and (100) planes of rGO but exhibiting higher intensity as compared to rGO.

The average crystallite size (D) is calculated for the most prominent peaks of rGO and NRGO using the Debye-Scherrer equation:

$$D = \frac{k\lambda}{\beta cos\theta} \tag{3}$$

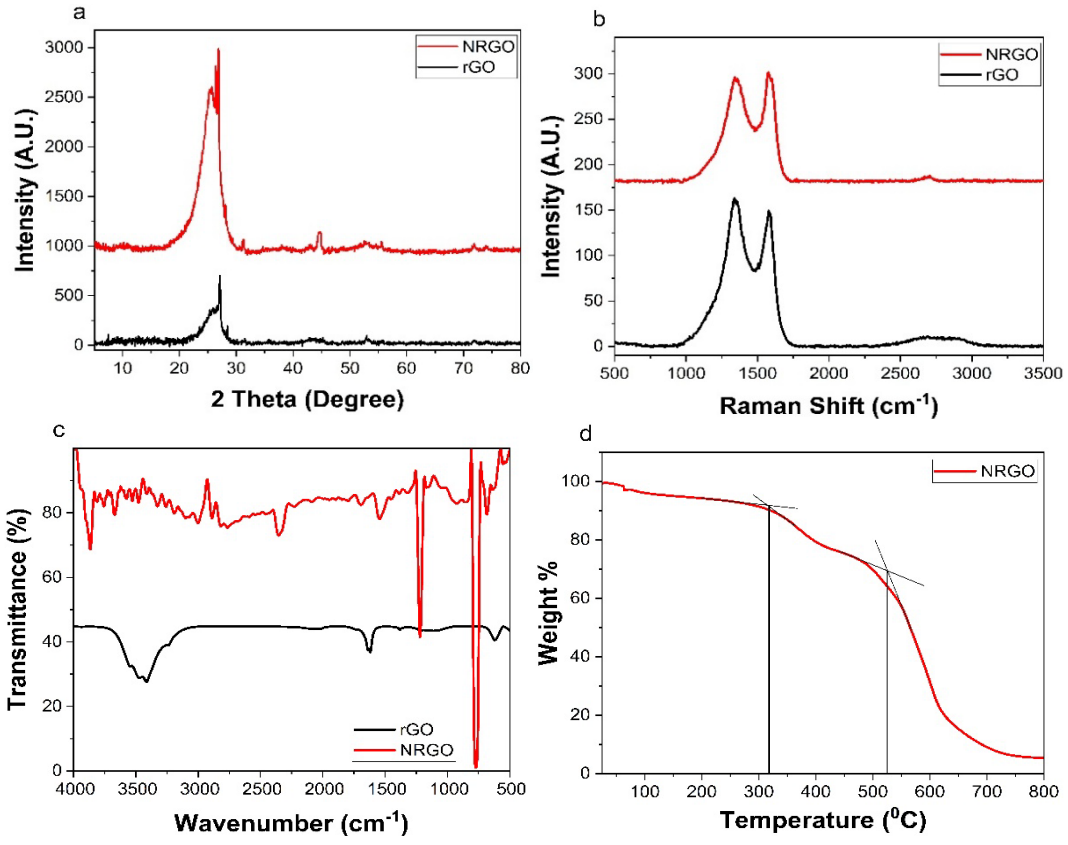

Fig. 3. (a) XRD spectra, (b) Raman Spectra, (c) FTIR of rGO and NRGO, and (d) TGA of NRGO under air atmosphere at a flow rate of 10 °C per minute.

Here k is a constant taken as 0.9 and β is full width at half maximum. Crystallinity index (C_I) is calculated for both samples using the following formula:

$$C_I = \frac{Area\ of\ crystalline\ peaks}{Area\ under\ all\ peaks\ (crystalline+amorphous)} * 100 \quad (4)$$

The various crystallographic parameters, along with crystallite size, are provided in Table 2. The d-spacing and crystallite size of rGO are comparable to NRGO. The crystallinity index of NRGO is better compared to rGO, which could be linked to a larger crystallite size for NRGO. The electrochemical performance of a fuel cell is also influenced by the crystallinity and surface area of the catalyst.

Table 2. Crystallographic parameters of rGO and NRGO.

Sample	2Theta(degrees)	FWHM (degrees)	d-spacing (Å)	Crystallite size(nm)	C_I (%)
RGO	25.52	3.898	3.49	2.10	52.79
NRGO	25.89	3.491	3.45	2.33	68.47

Given the versatility of Raman spectroscopy, it has become a characterizing method for carbon-based materials. The G band and D band are the two most important Raman bands of rGO, which are related to different phonon modes and different processes. In Figure 3(b), the G band for rGO appears at the frequency 1584 $cm^{-1,}$ which is related to the generation of E_2g phonon due to the vibration of the carbon atoms within the plane oriented towards the Brillouin zone center. The D band is centered at 1350 $cm^{-1,}$ which reflects the disorder-induced or defect-active mode related to sp^2 carbon contained in graphitic systems. The D and G bands for NRGO are centered at 1350 cm^{-1} and 1576 $cm^{-1,}$ respectively. A red shift in the G band is observed for NRGO, indicative of the restoration of sp^2 network in rGO, which is also justified by the intensity ratios of rGO (1.09) and NRGO (0.98). Apart from these two bands, additional broad bands around 2700 cm^{-1} to 2900 cm^{-1} called the 2D band and the D+G band, are observed. The 2D band is the second-order overtone effect of the D band. Further, the Tuinstra-Koenig relation demonstrates the relationship between the crystallite size obtained from XRD and the intensity ratio from Raman spectroscopy of disordered graphitic carbon [42]. According to the relation, crystallite size is inversely proportional to the intensity ratio. The crystallite size and intensity ratios of rGO are 2.10 nm and 1.09, and NRGO are 2.33 nm and 0.98. These results agree with the Tuinstra Koenig relation.

FTIR is a non-destructive technique that helps in determining the type of functional groups present in the given material. Figure 3(c) represents the FTIR spectrum of rGO and NRGO. The broad band centered at 3500 cm^{-1} in the spectrum of rGO is due to the presence of the hydroxyl group present in alcohol and carboxylic acid. The peak at 1624 cm^{-1} is the characteristic peak of C=C bond, and a less intense peak at 1374 cm^{-1} is due to C-H bending vibrations. A broad peak at 1104 cm^{-1} is caused by the C-O bond stretching of the alkoxy group. Additional peaks are present in the FTIR spectrum of NRGO due to the presence of nitrogen atoms in the rGO matrix. Peaks present at 3865 cm^{-1} and 3669 cm^{-1} are due to the primary amine stretch. Peaks at 2354 cm^{-1} and 1542 cm^{-1} correspond to the aliphatic nitrile group and C=N stretching vibrations. The presence of the amide group is confirmed by a peak at 1693 cm^{-1}. A prominent peak at 1219 cm^{-1} is due to the C-O-C epoxy group [43]. All the peaks below 1000 cm^{-1} suggest the presence of unsaturated carbon (C=C bond) and C-H wagging vibrations.

TGA was performed to study and analyze the stability of NRGO under air at a heating rate of 10 °C min^{-1}. Figure 3(d) shows the TGA curve of NRGO. Two stages of weight loss are observed in the graph. The first weight loss of 20% begins at 317 °C and can be ascribed to the removal of water molecules from NRGO. The second weight loss is observed at 524 °C because of the removal of oxygen present in the functional groups and burning of the carbon skeleton. TGA graph reveals that NRGO is a suitable material to fabricate electrodes for low-temperature fuel cell.

Surface morphology was studied using HRTEM and FESEM. Figure 4 shows the electron microscopy images. A sheet-like structure with random aggregations is observed from the FESEM image (Figure 4(a)). HRTEM images show the stacking of a few layers of doped reduced graphene oxide sheets. Stacking of layers of the prepared samples is also evident from the 2D band observed in Raman spectra. NRGO sheets exhibit a wrinkled surface incorporated during the reduction of carbonyl and carboxylic groups. Figure 4(c-g) represents the elemental mapping of NRGO, confirming the presence of carbon, oxygen, and successful doping of nitrogen. Energy dispersive X-ray analysis (EDX) depicts the elemental composition of NRGO (Figure 4(h)). The measured atomic percentages of C, O, and N are 85.22%, 10.77%, and 4.01%, respectively.

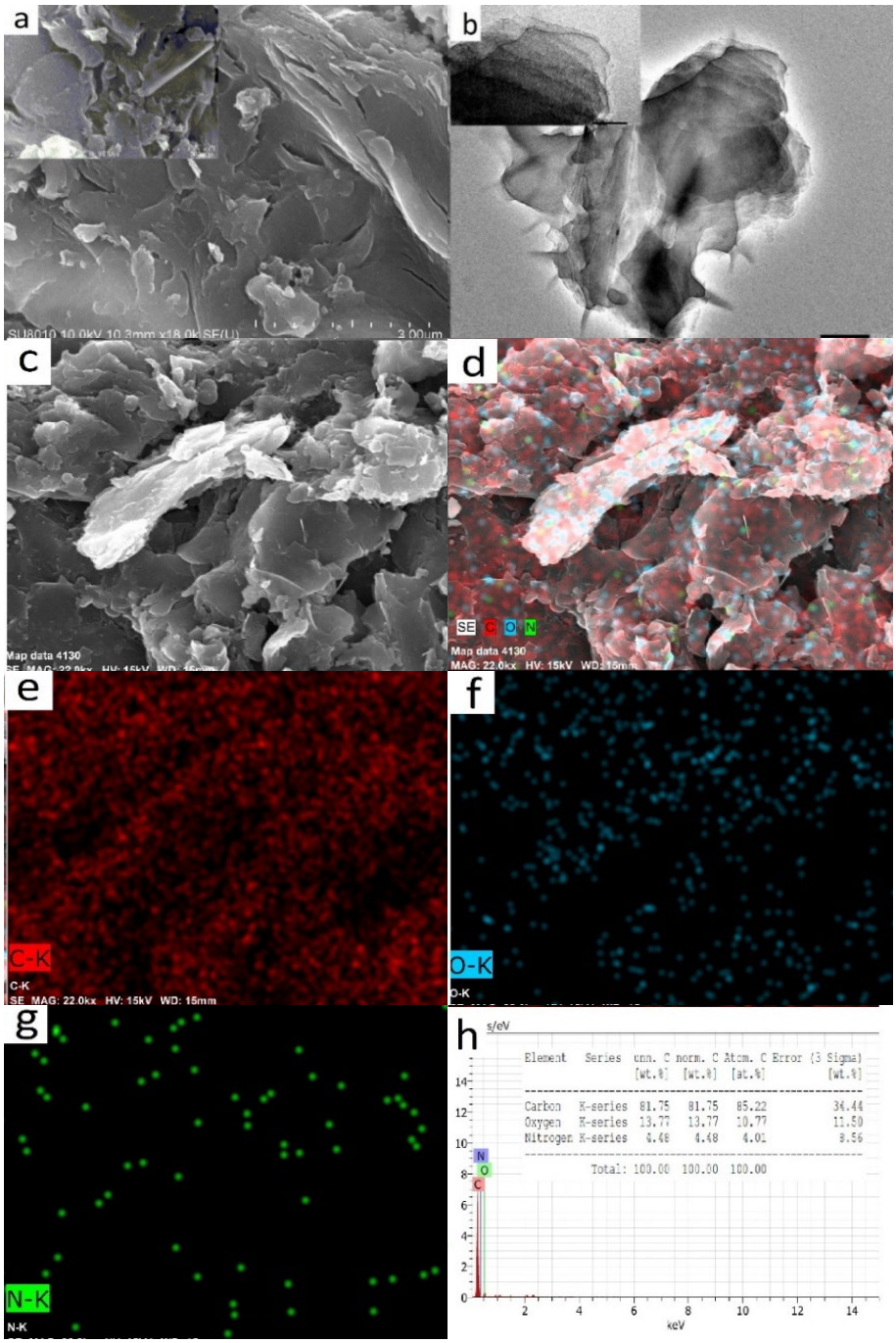

Fig. 4. Structure and morphology of prepared NRGO (a) FESEM (inset: higher magnification), (b) HRTEM (inset: higher magnification), (c-g) elemental mapping of NRGO confirming the presence of C, O, and N in the prepared samples, and (h) EDX mapping of NRGO.

3.3. Electrochemical characterization of NRGO

The prepared NRGO sample was electrochemically characterized by cyclic voltammetry using a three-electrode setup with a platinum electrode as the counter electrode and Ag/AgCl as a reference electrode. Figure 5(a) shows the CV curve for NRGO modified GCE in 1 M KOH solution at a sweep rate of 100 mVs^{-1}. There are no prominent peaks observed during the scan. During the anodic scan, OH^- ions from the electrolyte are adsorbed onto the surface of NRGO, leading to oxidation. The cathodic scan explains the desorption of OH^- ions. To test the catalytic activity of NRGO, ethanol is added to the KOH solution. Ethanol is one of the most studied fuels, as its oxidation is used as a simple model reaction for complex fuels used in fuel cells [44] NRGO nanosheets catalyze the ethanol oxidation reaction through the direct pathway. Figure 5(b) is the CV scan for ethanol electrooxidation in a mixture of 1 M KOH and 1 M ethanol on NRGO modified GCE at a scan rate of 100 mVs^{-1}. A distinct reduction peak has been observed at -0.5 V (vs Ag/AgCl). These observations are indicative of the efficient electrocatalytic activity of the prepared NRGO sheets towards ORR. The electrooxidation of ethanol manifests itself in the transfer of electrons from the alcohol to the electrocatalyst, which is in the form of an electrode. The adsorption mechanism, which is the interaction between molecules of alcohol and the surface of the catalyst, also affects the speed and selectivity of the reaction. The adsorption is categorized into two types, namely physisorption, where weak van der Waals bonds are involved, and chemisorption, where strong covalent bonds are created [45]. The adsorption energy denotes the affinity that exists between the adsorbates and the adsorbent surface and is defined as the energy difference before and after the adsorption, thus indicative of adsorption stability [46]. NRGO has good electrical conductivity and provides a large surface area for electrochemical reactions to occur. The processes of ethanol oxidation through NRGO catalysts primarily depend on the physical properties, such as exposed surface, composition, morphology, and reactivity. The most likely steps involved in the electrooxidation of ethanol are as follows: ethanol molecules are adsorbed on to the surface of the electrocatalyst, the adsorbed alcohol molecules are dehydrogenated and converted into CO and H_2O, CO is further oxidized into CO_2, and gaseous products CO_2 and H_2O are desorbed from the active sites of the catalyst [47].

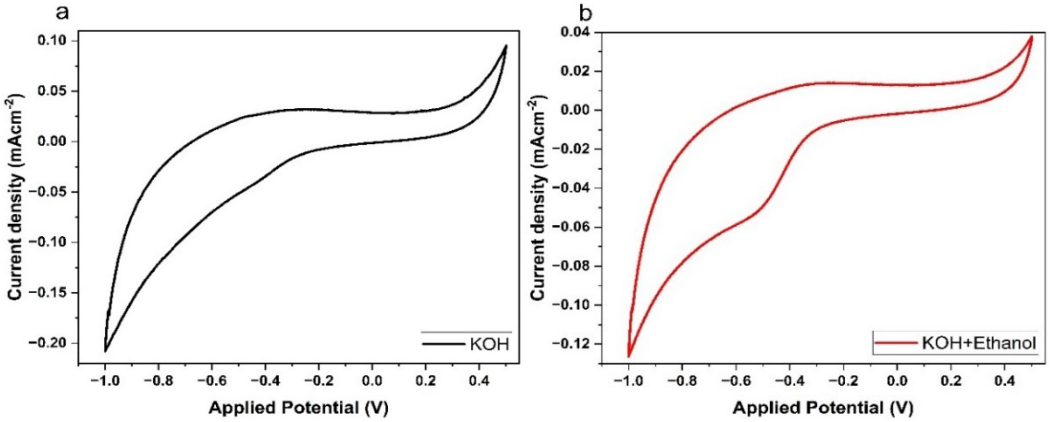

Fig. 5. Cyclic voltammetry curves (using three electrode electrochemical workstation with platinum as counter electrode, Ag/AgCl as reference electrode, and NRGO modified GCE as working electrode) in (a) 1M KOH, (b) 1M KOH and 1M ethanol at a scan rate of 100 mVs^{-1}.

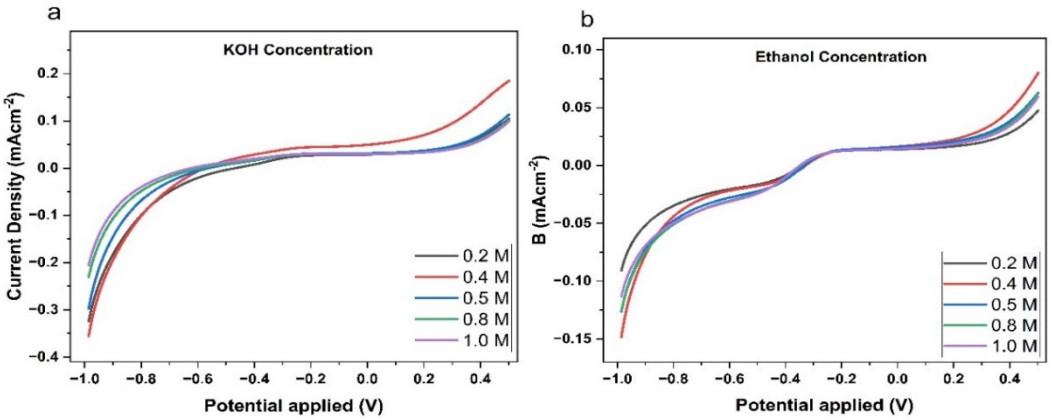

Fig. 6. Effect of fuel and electrolyte concentration on the forward cyclic voltammetry scans using NRGO as electrode at a scan rate of 100 mVs^{-1}.

Reduced graphene oxide-based electrodes are known for their excellent ability to catalyze and promote the electrooxidation of alcohols [48]. Figure 6(a) demonstrates the effect of varying the concentration of KOH on electrooxidation with a fixed ethanol concentration of 0.5 M. The anodic peak current density increases along with increasing concentrations of KOH, until it reaches a maximum at 0.4 M. Increasing concentration of KOH beyond this level is found to have a negative effect on current density. An increase in KOH concentration at the initial stage certainly assists in the adsorption and ethanol oxidation on the NRGO active sites. However, if KOH concentration is very high, there are too few active sites on the NRGO surface for ethanol electrooxidation, and increases in KOH concentration lead to domination of OH^- adsorption. In this scenario, there may be no difference between active sites for ethanol and OH^- on the NRGO surface. This competitive adsorption process leads to a reduction in active sites for ethanol. Figure 6(b) shows the CV curves for NRGO at different concentrations of ethanol. The efficiency and selectivity of the reaction can be estimated by the adsorption and dissociation process. Thus, adsorption of reactants and intermediates is vital for the electrocatalytic oxidation of ethanol. Hence, optimization of ethanol concentration is one of the critical factors. KOH concentration is kept constant at 0.5M while the concentration of alcohol is increased from 0.2 M to 1.0 M. As shown in Figure 6(b), NRGO demonstrates a maximum peak current density at 0.4M ethanol concentration, suggesting an optimum concentration for electrochemical activity. With further increase in the concentration of ethanol, saturation of electrochemically active sites with ethanol hinders the adsorption of hydroxyl groups [49].

Figure 7 shows the effect of varying scan rate on the peak current density, demonstrating the catalytic efficacy of NRGO with increasing scan rate. In the case of high scan rates, the diffusion process dominates the reaction rate, and therefore, there is an accumulation of electrolytic ions at the interface, while only a smaller fraction takes part in the charge transfer reaction [50]. A plot of peak current density (i_p) vs square root of scan rate ($\nu^{1/2}$) is linear, indicating the electrooxidation process to be diffusion-controlled. The electrochemical active surface area (ECSA) is calculated using the Randles-Sevcik equation:

$$i_p = 0.4463nFAC\left(\frac{nF\nu D}{RT}\right)^{1/2} \quad (5)$$

where n is the number of electrons exchanged in an electrochemical reaction; F and R are Faraday's and Gas constants; A, C, and D are ECSA, concentration, and diffusion constant of fuel, respectively. The ECSA calculated for prepared NRGO nanosheets is 22.08 cm^2g^{-1}.

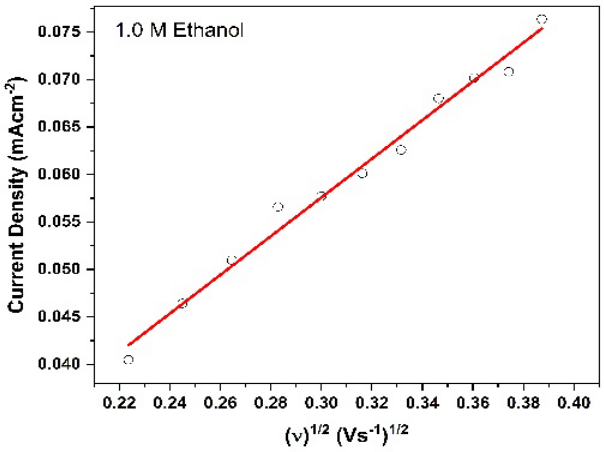

Fig. 7. Variation of peak current density against $v^{1/2}$. The linear relationship demonstrates the diffusion-controlled electrooxidation process.

4. Conclusion

Reduced graphene oxide and nitrogen-doped reduced graphene oxide are synthesized via a green route using electrochemical etching and hydrothermal synthesis methods. The prepared samples are structurally and optically characterized by XRD, FTIR, and Raman spectroscopy. The XRD results indicated the crystallite size of approximately 2 nm. The Raman spectra show two broad bands, viz D band and G band, specific to carbon materials. The thermal stability of the sample is determined using TGA. The morphology of the samples is examined through HRTEM and FESEM. NRGO has a multiple-stacked sheet-like structure with rough surfaces. Such structures are advantageous for catalytic activity. Electrochemical properties are studied using cyclic voltammetry, revealing ECSA of 22.08 cm^2g^{-1}. The dependence of catalytic activity and performance of NRGO on fuel and electrolyte concentration is also studied. It is observed that the optimum concentrations of both fuel and electrolyte are 0.4 M. These results indicate that the green synthesis method for the production of rGO and NRGO leads to a good electrochemical response in the oxidation of ethanol and acts as a potential method to produce electrodes for fuel cells at a commercial level.

Acknowledgements

This work is carried out in the Department of Physics, Panjab University. The authors are thankful to Central Instrumentation Lab, DAV, Sector-10, Chandigarh, for CV and FTIR facilities; RUSA Incubation Centre, Department of Physics, Panjab University, for CV facility; and SAIF, Mahatma Gandhi University, Kottayam, for Raman Spectroscopy facility.

References

[1] J. Brodny, M. Tutak, Science of The Total Environment, 808, 152052 (2022); https://doi.org/10.1016/j.scitotenv.2021.152052

[2] S. Nan, R. Tu, T. Li, J. Sun, H. Chen, Energy, 261, 125188 (2022); https://doi.org/10.1016/j.energy.2022.125188

[3] M. D. Sharma, N. Goyal, Journal of Ovonic Research, 14(1), 145-154(2018).

[4] A. Öztürk, R. G. Akay, S. Erkan, A. B. Yurtcan, Direct Liqiud Fuel Cells: Fundamentals. Advances and Future, Academic Press, 1-47, 2021; https://doi.org/10.1016/B978-0-12-818624-4.00001-7

[5] J. Garche, L. Jörissen, Electrochemical Soiety. Interface, 24(2), 39 (2015); https://doi.org/10.1149/2.F02152if
[6] F. Su, C. K. Poh, Z. Tian, G. Xu, G. Koh, Z. Wang, Z. Liu, J. Lin, Energy and Fuels, 24(7), 3727 (2010); https://doi.org/10.1021/ef901275q
[7] C. H. Sung, R Bopplea, J. W. Yoo, D. H. Lim, B. M. Moon, D. H. Kim, J. Y. Kim, Advanced Material Interfaces, 4(21) (2017); https://doi.org/10.1002/admi.201770107
[8] M. Yaldagard, M. Jahanshahi, N. Seghatoleslami, World Journal of Nano Scence and Engineering, 3(4), 121 (2013); https://doi.org/10.4236/wjnse.2013.34017
[9] J. Ma, L. Wang, X. Mu, Y. Cao, Journal of Colloid and Interface Science, 457, 102 (2015); https://doi.org/10.1016/j.jcis.2015.06.031
[10] J. C. Meier, C. Galeano, I. Katsounaros, A. A. Topalov, A. Kostka, F. Schüth, K. J. J. Mayrhofer, ACS Catalysis, 2(5), 832 (2012); https://doi.org/10.1021/cs300024h
[11] N. Mansor, J. Jia, T. Miller, T. Suter, A. B. Jorge, C. Gibbs, P. R. Shearing, P. F. McMillan, C. Mattevi, M. Shaffer, D. J. L. Brett, ECS Transactions, 75(14), 885 (2016); https://doi.org/10.1149/07514.0885ecst
[12] T. Merzdorf, S. Kühl, A. Herzog, P. Strasser, ECS Transactions, 92(8), 547 (2019); https://doi.org/10.1149/09208.0547ecst
[13] H. Yang, X. Zhang, H. Zou, Z. Yu, S. Li, J. Sun, S. Chen, J. Jin, J. Ma, ACS Sustainable Chememistry and Engineering, 6(6), 7918 (2018); https://doi.org/10.1021/acssuschemeng.8b01157
[14] S. Samantaray, D. Mohanty, S. K. Satpathy, I. M. Hung, Molecules, 29(12), 2937 (2024); https://doi.org/10.3390/molecules29122937
[15] X. Qiu, P. Wu, L. Xu, Y. Tang, J. M. Lee, Advanced Materials Interfaces, 2(18), 1500321 (2015); https://doi.org/10.1002/admi.201500321
[16] T. T. Luyen, T. V. Hoang, Vietnam Journal of Catalysis and Adsorption, 12(2), 81 (2023); https://doi.org/10.51316/jca.2023.034
[17] Y. Xiang, L. Xin, J. Hu, C. Li, J. Qi, Y. Hou, X. Wei, Crystals, 11(1), 47 (2021); https://doi.org/10.3390/cryst11010047
[18] G. Kim, J. Lee, T. Liu, C. P. Grey, Journal of Physical Chemistry C, 125(19), 10558 (2021); https://doi.org/10.1021/acs.jpcc.1c02669
[19] Y. Jee, A. Karimaghaloo, A. Macedo Andrade, H. Moon, Y. Li, J.-W. Han, S. Ji, H. Ishihara, P.-C. Su, S. W. Cha, V. C. Tung, M. H. Lee, Fuel Cells, 17(3), 344 (2017); https://doi.org/10.1002/fuce.201600169
[20] C. P. Deming, R. Mercado, J. E. Lu, V. Gadiraju, M. Khan, S. Chen, ACS Sustainable Chemistry and Engineering, 4(12), 6580 (2016); https://doi.org/10.1021/acssuschemeng.6b01476
[21] R. Imran Jafri, N. Rajalakshmi, S. Ramaprabhu, Journal of Materials Chemistry, 20(34), 7114 (2010); https://doi.org/10.1039/c0jm00467g
[22] D. W. Chang, H. J. Choi, J. B. Baek, Journal of Materials Chemistry A, 3(14), 7659 (2015); https://doi.org/10.1039/C4TA07035F
[23] Z. Li, X. Li, Y. Zong, G. Tan, Y. Sun, Y. Lan, M. He, Z. Ren, X. Zheng, Carbon, 115, 493 (2017); https://doi.org/10.1016/j.carbon.2017.01.036
[24] G. Zhang, W. Lu, F. Cao, Z. Xiao, X. Zheng, Journal of Power Sources, 302, 114 (2016); https://doi.org/10.1016/j.jpowsour.2015.10.055
[25] S. Guo, Y. Yang, N. Liu, S. Qiao, H. Huang, Y. Liu, and Z. Kang, Science Bulletin, 61(1), 68 (2016); https://doi.org/10.1007/s11434-015-0978-6
[26] F. Bai, H. Huang, Y. Tan, C. Hou, P. Zhang, Electrochimica Acta, 176, 280 (2015); https://doi.org/10.1016/j.electacta.2015.07.010
[27] D. He, Y. Jiang, H. Lv, M. Pan, S. Mu, Applied Catalysis B: Environmental, 132, 379 (2013); https://doi.org/10.1016/j.apcatb.2012.12.005
[28] K. Kakaei, M. Rahnavardi, Renewable Energy, 163, 1277 (2021); https://doi.org/10.1016/j.renene.2020.09.043
[29] L. Du, V. Prabhakaran, X. Xie, S. Park, Y. Wang, Y. Shao, Advanced Materials, 33(6), 1908232 (2021); https://doi.org/10.1002/adma.201908232
[30] C. Lafforgue, A. Zadick, L. Dubau, F. Maillard, M. Chatenet, Fuel Cells, 18(3), 229 (2018); https://doi.org/10.1002/fuce.201700094

[31] Z. J. Lu, S. J. Bao, Y. T. Gou, C. J. Cai, C. C. Ji, M. W. Xu, J. Song, R. Wang, RSC Advances, 3(12), 3990 (2013); https://doi.org/10.1039/c3ra22161j

[32] A. Farzaneh, E. K. Goharshadi, H. Gharibi, N. Saghatoleslami, H. Ahmadzadeh, Electrochimica Acta, 306, 220 (2019); https://doi.org/10.1016/j.electacta.2019.03.120

[33] A. Farzaneh, N. Saghatoleslami, E. K. Goharshadi, H. Gharibi, H. Ahmadzadeh, Electrochimica Acta, 222, 608 (2016); https://doi.org/10.1016/j.electacta.2016.11.015

[34] A. A. Nafiey, P. Subramanian, A. Addad, B. Sieber, S. Szunerits, R. Boukherroub, ECS Journal of Solid State Science and Technology, 5(8), M3060 (2016); https://doi.org/10.1149/2.0121608jss

[35] N. Singh, P. Siwatch, J. Kaushal, J. Sharma, S. K. Tripathi, Journal of Solid State Chemistry, 291, 121537 (2020); https://doi.org/10.1016/j.jssc.2020.121537

[36] M. Alpha, U. E. Uno, K. U. Isah, U. Ahmadu, Nigerian Jpurnal of Technology, 38(4), 997 (2019); https://doi.org/10.4314/njt.v38i4.24

[37] O. A. Abdulrazzaq, S. K. Abdulridha, D. F. Ali, H. Al-Qarishey, Iraqi Journal of Industrial Research, 10(2), 57 (2023); https://doi.org/10.53523/ijoirVol10I2ID292

[38] V. Sharma, Y. Jain, M. Kumari, R. Gupta, S. K. Sharma, K. Sachdev, Macromolecular Symposia, 376(1), 1700006 (2017); https://doi.org/10.1002/masy.201700006

[39] J. Światowska, V. Lair, C. Pereira-Nabais, G. Cote, P. Marcus, A. Chagnes, Applied Surface Science, 257(22), 9110 (2011); https://doi.org/10.1016/j.apsusc.2011.05.108

[40] C. N. Barnakov, G. P. Khokhlova, A. N. Popova, S. A. Sozinov, Z. R. Ismagilov, Eurasian Chemico-Technological Journal, 17(2), 87 (2015); https://doi.org/10.18321/ectj198

[41] L. Stobinski, B. Lesiak, A. Melolepszy, B. Mierzwa, J. Zemek, P. Jiricek, I. bieloshapka, Journal of Electron Spectroscopy and Related Phenomena, 195, 145 (2014); https://doi.org/10.1016/j.elspec.2014.07.003

[42] A. Cuesta, P. Dhamelincourt, J. Laureyns, A. Martínez-Alonso, J. M. D. Tascón, Journal of Materials Chemistry, 8(12), 2875 (1998); https://doi.org/10.1039/a805841e

[43] A. Bayu, D. Nandiyanto, R. Oktiani, R. Ragadhita, Indonesian Journal of Science and Technology, 4(1), 97 (2019); https://doi.org/10.17509/ijost.v4i1.15806

[44] K. Bhunia, S. Khilari, D. Pradhan, ACS Sustainable Chemistry and Engineering, 6(6), 7769 (2018); https://doi.org/10.1021/acssuschemeng.8b00721

[45] K. R. Chaturvedi, T. Sharma, Journal of Petroleum Science and Engineering, 194, 107499 (2020); https://doi.org/10.1016/j.petrol.2020.107499

[46] Z. Liu, Q. Wang, Q. Kong, X. Tong, S. Wu, N. Zong, R. Xu, L. Yang, Sustainability, 15(16), 12240 (2023); https://doi.org/10.3390/su151612240

[47] A. Ehsani, A. A. Heidari, R. Asgari, The Chem.ical Record, 19(11), 2341 (2019); https://doi.org/10.1002/tcr.201800176

[48] R. Rajeev, B. Sharma, A. T. Mathew, L. George, S. Y. N, A. Varghese, Journal of the Electrochemical Society, 167(13), 136508 (2020); https://doi.org/10.1149/1945-7111/abb9d0

[49] Y. S. Li, T. S. Zhao, Z. X. Liang, Journal of Power Sources, 187(2), 387 (2009); https://doi.org/10.1016/j.jpowsour.2008.10.132

[50] N. Elgrishi, K. J. Rountree, B. D. McCarthy, E. S. Rountree, T. T. Eisenhart, J. L. Dempsey, Journal of Chemical Education, 95(2), 197 (2018); https://doi.org/10.1021/acs.jchemed.7b00361